JOURNAL OF MATERIALS SCIENCE 30 (1995) 5531–5536

Hot hardness of Si_3N_4-based materials

R. F. SILVA, J. M. VIEIRA
Departamento Eng. Cerâmica e Vidro, Universidade de Aveiro, 3800 Aveiro, Portugal

The Vickers hardness of dense Si_3N_4 ceramics of the Si–Ce–Al–O–N system was investigated from room temperature to 1200 °C. A sloppy decrease of hot hardness occurred above 850–900° C. A compensation law was observed between the pre-exponential factors of the hot-hardness dependence on the reciprocal of absolute temperature, and the values of the activation energy of hardness. This relationship shows that the low-temperature deformation mechanism, such as microplasticity, is competing in parallel with a grain-boundary diffusion-controlled creep process in the high-temperature range.

1. Introduction

Hot hardness is a key property of hard materials whenever friction or abrasion cause the contact surface temperature to approach 1000 °C or above. Among the potential applications of the Si_3N_4 ceramics, their use as cutting inserts is progressively spreading in industry. Cutting tools are subjected to mechanical and thermal stresses that induce wear, and chemical wear. The stress fields are characterized by compressive stresses that are highly confined to the microasperity contacts, which are closely reproduced by microhardness tests.

In high-speed cutting with ceramic tools, the development of heat increases the surface temperature to 1200 °C [1], where the mechanical properties of polycrystalline ceramics are degraded by grain-boundary processes [2–5]. Thus, it is assumed that hardness tests at high temperature are a close approximation of the thermomechanics of the cutting process.

The results for high-temperature hardness for different silicon nitride-based ceramics show that a drastic decrease of hardness above 750–900 °C, as the result of softening of the intergranular glassy layer, is caused by the sintering aids for Si_3N_4 [6–9]. The composition and amount of additives in the nitride system have a strong influence on hot hardness, the rare-earth oxides-based dopants [6] and nitrogen-enriched compositions [8] giving the best results.

If no amorphous intergranular layer is present, which is found only if hot isostatic pressing without additives, or Si_3N_4 chemical vapour deposition are used as processing routes, the room-temperature hardness can be retained almost up to high temperatures [7–11]. A single value of 19.1 GPa was determined at 1500 °C [7].

In this paper, hot-hardness results for cutting-tool materials of the Si–Ce–Al–O–N system are quantitatively correlated to the deformation mechanisms and microstructural properties of the Si_3N_4 ceramics, by using the compensation law [12, 13]. This law has been applied to the electrical conductivity of ceramics at high temperature [12], to the tracer diffusion coefficients of Al_2O_3 [13], and to the volume diffusion coefficients and the effective diffusion coefficients for creep, hot-pressing and sintering of MgO [14].

2. Experimental procedure

The powder batches for hot pressing were prepared by wet mixing weighted amounts of Si_3N_4, CeO_2 and AlN or Al_2O_3 powders. The theoretical composition of the batches is given in Table 1. Cylindrical pellets were uniaxially hot-pressed at 20–30 MPa applied pressure, and dwell times from 5–120 min, in the range 1500–1750 °C, Table II. Sample 2CeAl2 was submitted to a post hot isostatic pressing (HIP) treatment at 1750 °C/60 min/100 MPa. The bulk density was measured by Archimedes' method with mercury. Phase composition was determined by X-ray diffraction (Philips PW 1729/1840) using the method described by Gazzara and Messier [15], by measuring the heights of the $\alpha(2\,1\,0)$, $\alpha(2\,0\,1)$, $\beta(2\,1\,0)$, $\beta(1\,0\,1)$ and $\beta(2\,0\,0)$ lines.

The surfaces parallel to the hot-pressing direction were polished on 1 μm diamond paste before the hardness measurements. Grain size, G, the cubic root of the grain volume ($G^3 = 3 \times 3^{1/2}/2\, ld^2$), the two-dimensional grain aspect ratio, $AR = l/d$ (l being the grain length and d the grain diameter) were determined from cord-length measurements on scanning electron (JSM 35C) micrographs of polished and chemically etched surfaces, according to the procedures established for hexagonal prisms [16] and the a_{95} aspect ratio parameter of elongated particles [17]. The room-temperature hardness was measured by using a Vickers indentor with the 9.8 N load, loading speed of 0.017 ms^{-1} and 15 s indentation time (Shimadzu M). The hardness is the average of 20 indentations for each sample.

Hot-hardness experiments were carried out in a temperature controlled microhardness tester operating under vacuum (10^{-5}–10^{-6} mbar). Vickers hot-hardness was measured by using the 4.9 N load and 15 s indentation time. Hardness tests were performed from room temperature up to 1200 °C in steps of 100

0022–2461

TABLE I Theoretical composition of the Si_3N_4 batches

Batch	Si_3N_4 (wt %)	CeO_2 (wt %)	Al (wt %)	Al_2O_3 (wt %)
Ce1	97.5[a]	2.5[c]	–	–
Ce2	95[a]	5[c]	–	–
Ce3	90[a]	10[c]	–	–
CeAl1	89[b]	5[c]	6[d]	–
CeAl2	83.4[b]	10[c]	6.6[d]	–
Al1	95[a]	–	–	5[e]

[a]HcStrack LC10. [b]HcStrack LC12. [c]Fluka puriss. [d]HcStrack grade C. [e]Union Carbide LindeA.

TABLE II Relative densities, hot-pressing conditions and room-temperature microhardness (standard deviation in brackets) for Si_3N_4 samples

Sample	ρ	T(°C)/t(min)/P(MPa)	H(GPa)
1Ce1	0.942	1750/45/30	12.9(0.9)
1Ce2	0.982	1750/90/20	13.9(0.4)
2Ce2	0.948	1700/90/20	11.8(0.4)
1Ce3	0.945	1750/15/30	11.0(0.5)
1CeAl1	0.998	1500/60/30	19.7(0.7)
2CeAl1	0.998	1550/60/30	19.2(0.5)
3CeAl1	1	1600/60/30	18.3(0.5)
4CeAl1	1	1750/15/30	16.7(0.4)
1CeAl2	0.993	1650/5/30	15.7(0.3)
2CeAl2	0.992	1750/60/100	15.0(0.4)
1Al1	0.978	1700/120/20	16.1(0.5)

or 200 °C. Indentation diagonal lengths were measured on the cooled sample, outside the apparatus, using an optical microscope. The hot-hardness is the average of five indentations for each temperature. For the hardest α-Si_3N_4 samples (batch CeAl1), the small dimensions of the indentor impression below 800 °C were difficult to measure, as they became comparable to the thermal etching features of the surface.

3. Results and discussion

The hot-pressing conditions, the relative density, ρ, and room-temperature microhardness, H, for the Si_3N_4 samples, are given in Table II. Microstructural parameters l, d, G and AR and crystalline-phase amounts of the CeAl1 batch are given in Table III. Vickers hardness values that were obtained with the hot-hardness apparatus are presented in Table IV. The standard deviation of each hardness value is less than 0.05.

TABLE III Phase amount and morphological parameters of the CeAl1 samples

Sample	α-Si_3N_4 (wt %)	β-Si_3N_4 (wt %)	l(μm)	d(μm)	G(μm^3)	AR
1CeAl1	77.3	22.7	0.66	0.31	0.25	2.1
2CeAl1	64.8	35.2	1.13	0.27	0.29	4.2
3CeAl1	43.1	56.9	1.33	0.29	0.33	4.6
4CeAl1	21.0	79.0	3.46	0.36	0.67	9.5

Hot-hardness results can be presented by a semi-logarithmic plot of hardness against temperature [18, 19]. However, the contribution of thermally activated deformation processes makes the Arrhenius plot of $\ln H$ versus $1/T$ presumably more adequate for presenting the dependence of hardness of polycrystalline ceramics on temperature [20]. Potential changes of hot-hardness are made clear and quantitative comparison of hot-hardness data with the parameters of known deformation mechanisms becomes possible.

The Arrhenius plots of H for the present results are shown in Fig. 1. The pre-exponential factors and the activation energies for H that were calculated by linear fitting of $H = A^* \exp(Q_H/RT)$ to the experimental data, where Q_H is the activation energy of hardness, are given in Table V. Room-temperature hardness was used in the best linear fitting calculation of H only if there were too few data points in the low-temperature range, $400\,°C \leqslant T \leqslant 900\,°C$.

Brittle materials exhibit plastic deformation at room temperature under the stress field that is generated by the indentor: a hydrostatic, highly confined compression combined with a localized, large shear stress [21, 22]. Although tensile microfracture from crack nucelation by plastic deformation and extensive crack propagation from the elastic/plastic boundary is possible, microplasticity is reported to be the dominant deformation mode [19, 22]. As the crack propagation energy is much less than that of plastic yielding [23], plasticity takes most of the indentation work.

Such permanently strained impressions result from different deformation mechanisms [3–5]. These mechanisms have been classified into two broad classes

TABLE IV Hot hardness (GPa) of Si_3N_4-based materials

Sample	RT	400 °C	600 °C	800 °C	900 °C	1000 °C	1100 °C	1200 °C
1Ce1	14.2	11.7	9.7	8.4	7.9	7.8	7.2	6.3
1Ce2	15.6	13.1	11.1	9.9	9.0	8.1	7.4	6.8
2Ce2	12.4	9.7	8.9	8.0	7.6	7.2	6.3	5.6
1Ce3	11.8	9.0	8.6	7.5	7.0	6.3	5.0	4.6
1CeAl1	–	–	–	17.7	15.9	13.9	11.4	9.5
2CeAl1	–	–	–	15.8	14.2	12.9	10.9	9.0
3CeAl1	–	–	–	14.5	13.8	12.8	9.8	9.7
4CeAl1	18.0	14.4	13.0	12.1	12.1	10.7	9.7	9.2
1CeAl2	–	–	–	12.6	10.6	9.3	7.8	7.0
2CeAl2	15.0	14.8	13.0	11.8	10.7	8.3	6.7	5.9
1Al1	14.9	12.6	12.1	10.8	10.2	9.8	9.6	9.2

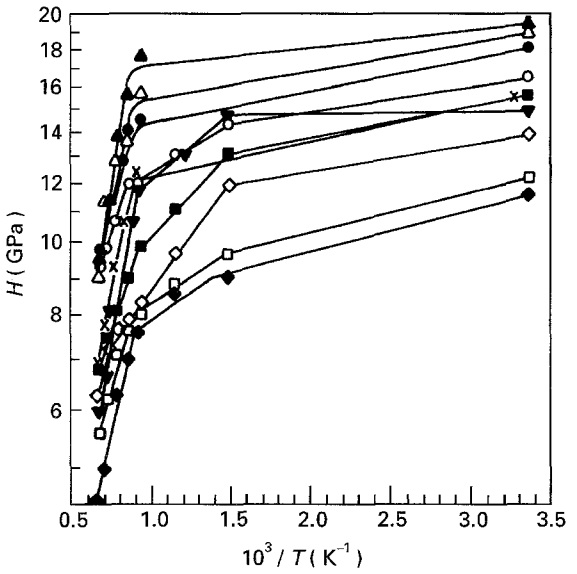

Figure 1 Arrhenius plots of the hot-hardness of Si_3N_4 ceramics from room temperature to 1200° C (■) 1Ce2, (□) 2Ce2, (◆) 1Ce3, (◇) 1Ce1, (▲) 1CeAl1, (△) 2CeAl1, (●) 3CeAl1, (○) 4CeAl1, (×) 1CeAl2, (▼) 2CeAl2.

TABLE V Parameters of curve-fitting of hardness to temperature, according to the Arrhenius equation $H = A^* \exp(Q_H/RT)$

Sample	Temp. range (°C)	A^*(GPa)	$Q_H(Q_{H1})$ (kJ mol^{-1})
1Ce1	400–900	4.7	5.1
	1000–1200	1.5	17.3
1Ce2	400–800	6.2	4.2
	900–1200	2.2	13.6
2Ce2	400–800	5.9	2.8
	900–1200	1.6	15.2
1Ce3	400–800	5.8	2.5
	900–1200	0.8	21.7
1CeAl1	RT–900	15.8	0.6
	900–1200	1.3	24.7(51.6)
2CeAl1	RT–900	13.7	0.8
	900–1200	1.6	21.8(52.9)
3CeAl1	RT–900	12.9	0.9
	900–1200	2.3	17.6(46.0)
4CeAl1	400–800	9.1	2.6
	900–1200	3.1	13.1(47.5)
1CeAl2	RT–900	10.3	1.0
	900–1200	1.3	20.5
2CeAl2	400–800	8.0	3.4
	900–1200	5.5	28.7
1Al1	RT–600	10.9	0.8
	800–1200	6.1	5.0

[2,21]: (a) grain processes (dislocation motion and twinning), and (b) grain-boundary processes such as grain-boundary dislocation activity and diffusional flow. Deformation mechanisms are described by rate equations that can be simplified to the major dependencies of their strain rate on temperature, applied stress and grain size.

The temperature dependence of hot hardness of Si_3N_4 materials shows two ranges: the first range goes from room temperature to 800–900 °C (Fig. 1), or from room temperature to 750 °C for the MgO-doped samples (Fig. 2), and the second range prevails above these temperatures. The hot hardness in the second range

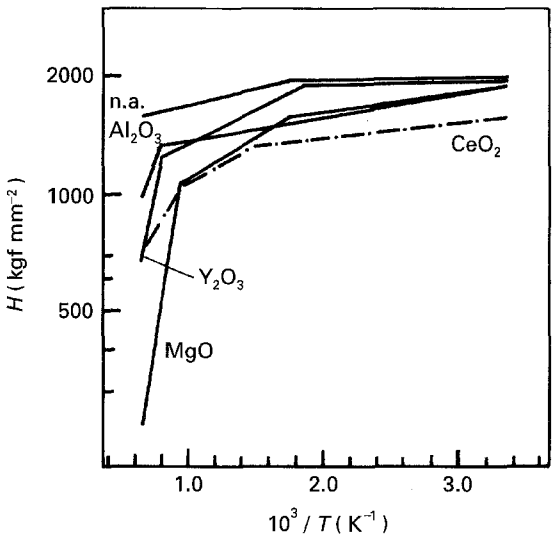

Figure 2 Hot-hardness values for Si_3N_4 with approximately equal amounts (4–5%) of different sintering aids [15] (n.a.-without sintering additives).

has a much stronger temperature dependence than in the first range. Softening of the intergranular phase of the Si_3N_4 has been reported at these temperatures [6].

The mechanical strength is changed by the composition of the secondary phase, as can be seen by comparing the hardness curves, Fig. 2, of the following systems: high-pressure hot-pressed Si_3N_4 with no additives [6], 5%CeO_2–Si_3N_4 (sample 1Ce2), 4%Al_2O_3–Si_3N_4 [6], 4%MgO–Si_3N_4 [6] and 5% Y_2O_3–Si_3N_4 [6]. Hardness is almost retained up to 1100 °C for the first system, when the glassy layer between the Si_3N_4 grains is absent. The Al_2O_3-doped sample shows the highest values of hardness at high temperatures when compared to those with other oxide additions. In this system, a transient liquid phase develops between the Si_3N_4 grains thus lowering the final glassy phase volume and increasing the hardness. The results for the CeO_2-doped sample, 1Ce2, are similar to the microhardness values for the other rare-earth-doped material (4%Y_2O_3–Si_3N_4), denoting a comparable influence of the intergranular amorphous layer on the high-temperature mechanical behaviour.

Boundary-phase refractoriness is improved for CeAl1 samples in comparison to Ce2 samples, Fig. 1. The viscosity of the amorphous phase increases by nitrogen enrichment [24–26]. Because AlN was used as a sintering aid, the highest values of hot hardness at 1200 °C were observed in the CeAl1 samples (≈10 GPa).

In the high-temperature range, the amount of second phase has a remarkable effect in decreasing hardness, as can be seen from the comparison of the slopes, Fig. 1, of equally densified samples 1Ce1, 2Ce2 and 1Ce3. The same trend was found for the Y_2O_3–Si_3N_4 system [6]. This is explained by the dependence of the diffusional flow rate on the grain-boundary film thickness, which is expected to be more effective at high temperatures.

The values of the activation energy of hardness, Q_H, in the low-temperature range, are between 0.6 and

5.1 kJ mol^{-1}, Table V, the lowest values of Q_H being observed for the hardest samples, batch CeAl1. This range of values of Q_H is in close agreement with other data on silicon nitride-based materials [21]. In the high-temperature range, the activation energy of hardness is much higher. In this temperature range, diffusion creep mechanisms are expected to control deformation, the corresponding rate equations being given as [27]

$$d\varepsilon/dt = A\sigma^m \exp(-Q/RT) \quad (1)$$

where $d\varepsilon/dt$ is the strain rate, σ the applied stress and Q the activation energy for the creep mechanism.

The dependence of hardness, H, on temperature, T, at constant loading time, t, and temperature, T, can be calculated from Equation 1 as [21]

$$H = (A'/t)^{1/m} \exp(Q/mRT) \quad (2)$$

where $(A'/t)^{1/m}$ is constant. Equation 2 shows that the hardness activation energy is decreased by a factor of m in comparison to the true activation energy of the deformation mechanism. The values of stress exponents for creep, m, go up to a value of 5 [28]. Owing to the high stresses that are created under the indentor, it has been found that m should be even higher for hardness, $m \approx 8$–13 [29–31]. The activation energies at high temperatures in Table V will be in the range of 50–250 kJ mol^{-1}, after being multiplied by $m = 10$. Such values of Q are not amenable to a direct comparison with known values of the activation energy of the creep mechanisms of Si_3N_4 [27].

In order to clarify this deviation of the activation energies and the full set of different values of Q_H found for a given batch, such as CeAl1, which is unexpected because as a first approach, the intergranular paths for diffusion-controlled deformation are chemically identical, the morphological parameters of the CeAl1 samples were also measured, Table III. In a previous paper [32], room-temperature dependence of hardness on the composition, amount of intergranular phases, α–β Si_3N_4 phase content, residual porosity, grain size and grain aspect ratio, was investigated. As the result of the combination of morphological features and solid-phase volume fractions, room-temperature hardness decreases within the batch CeAl1 from sample 1CeAl1 to sample 4CeAl1, Table II.

The plot of ln $1/A^*$ versus Q_H for the high-temperature hardness (900–1200 °C) shows a linear relationship for these samples, Fig. 3. The reciprocals of the pre-exponential factors of hardness, calculated from data in Table V, were used as diffusivity related parameters in order to apply the analysis that results from the compensation law [12, 13].

The best linear fitting to the data corresponding to CeAl1 samples, with a correlation coefficient of (corr = 0.997), yields

$$\ln 1/A^* = 7.8 \times 10^{-2} Q_H - 2.2 \quad (3)$$

with the units of Fig. 3.

The compensation law has been consistently applied to the study of diffusion data and to the transport of matter in sintering and high-temperature creep of ceramics [12–14]. The linear relationship resulting from the compensation law, Fig. 3, may represent a combination of two thermally activated processes, either as independent (parallel) mechanisms or dependent (serial) mechanisms [13].

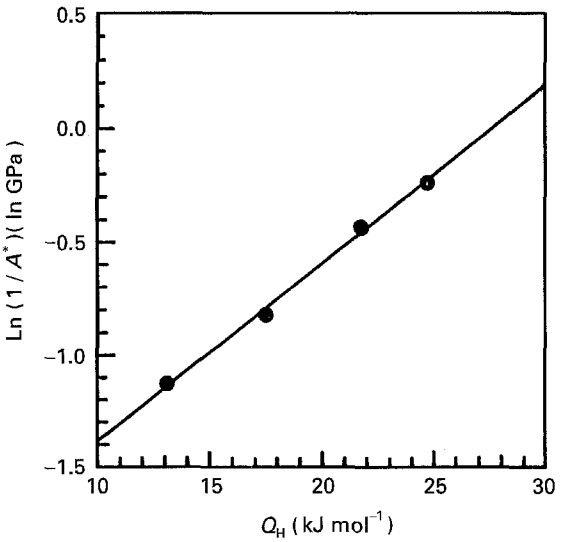

Figure 3 Compensation law as applied to hot-hardness of the Si_3N_4 ceramics in the Si–Ce–Al–O–N system.

Because the values of the high-temperature activation energies, Q_H, Table V, are determined in a region of transition from grain process-controlled hardness to the grain boundary-process control, we question if they resulted from a parallel contribution (or a serial contribution) of a low deformation mechanism to the high-temperature creep processes of hardness. Data confirm that a parallel contribution is present, as described below.

The grain-boundary diffusion mechanism will have an activation energy, Q_1, and a pre-exponential factor, D_{10}. By using the following expression [13] for parallel mechanisms

$$\ln D_0 - Q_H/RT = D_{20} - Q_2/RT - \ln[(Q_1 - Q)/(Q_1 - Q_2)] \quad (4)$$

and the values of D_{20} and Q_2 from the data corresponding to the low-temperature range in Table V, the values of Q_1 in Table V are obtained. The values of Q_1 for the different samples of the CeAl1 batch are very close together, the average value being $Q_1 =$ 49.5 kJ mol^{-1}. If Q_H is multiplied by the factor $m \approx 7$, physical consistency is achieved between the present results of the compensation law of hardness and the magnitude of the activation energy (353 kJ mol^{-1}) for the Si/N grain-boundary diffusion measured from the grain size-compensated densification rate in the intermediate stage of pressure sintering [33]. Activation energy for the creep of materials with the present composition was not determined but it will probably be higher than the reported value of Q from densification, as the residual intergranular phase which controls mechanical behaviour becomes more refractory than the transient fluid that assists liquid-phase sintering.

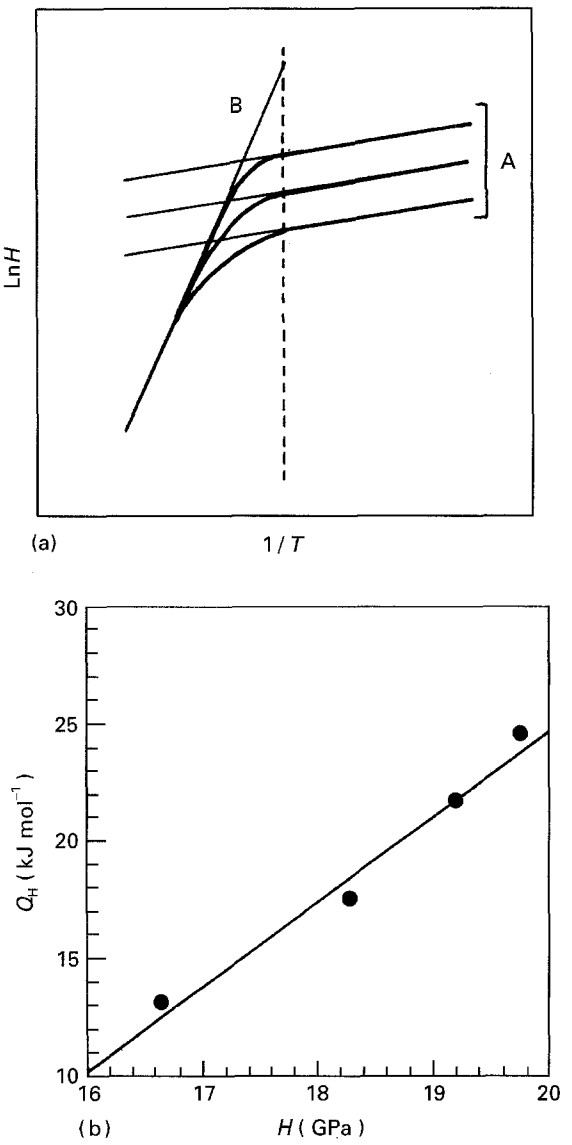

Figure 4 (a) Schematic representation of the dependence of the high-temperature hardness fall on values of room-temperature hardness; (b) dependence of the hardness activation energy on the room-temperature hardness for batch CeAl1.

Fig. 4a is a schematic representation of the hot hardness of three different materials with different room-temperature hardnesses (regime A) and a similar high-temperature fall (regime B). If the thermally activated mechanism, B, becomes active above a certain temperature, samples with high room-temperature hardness will show the highest decrease in hardness in the high-temperature range. This effect is seen in Fig. 1 for the experimental results. When Q_H is plotted against room-temperature hardness (Fig. 4b), a linear dependence of Q_H on H, will be observed, thereby confirming the tendency postulated by the analysis based on the compensation law.

4. Conclusions

Hot-hardness measurements on Si_3N_4-based materials have shown two distinct deformation mechanisms in the temperature range from room temperature to 1200 °C. From room temperature to 900 °C, microplasticity is expected to be the dominant deformation mechanism of the brittle Si_3N_4 ceramics under the stress field of the indentor. From the analysis of the present hardness data using the compensation law, the low-temperature mechanisms is found to compete in the second, 900–1200 °C, range with a grain-boundary creep mechanism, a diffusion-like flow mechanism. The argument is supported by observation of a correlation between the decrease in hardness and the corresponding room-temperature values of hardness, and by the single value of Q that is calculated from the activation energies of hardness.

Microhardness of Si_3N_4-based materials is also dependent on the amount and composition of intergranular phase. Nitrogen-enrichment of the amorphous phase and minor additions results in the highest values of H at high temperature. The changes of hardness that are due to morphological properties alone can be incorporated into the present framework of analysis of hot hardness.

Acknowledgements

We thank the Department of Metallurgy and Science of Materials, University of Oxford, UK, and in particular Dr Steve Roberts, for the use of the hot hardness apparatus. The financial support from JNICT and Minas e Metalurgia under research contract 87/80 MATR is also gratefully acknowledged.

References

1. S. T. BULJAN and S. F. WAYNE, *Wear* **133** (1989) 309.
2. P. C. DOKKO and J. A. PASK, *Mater. Sci. Eng.* **25** (1976) 77.
3. J. FROST and M. F. ASHBY, "Deformation mechanism maps" (Pergamon Press, New York, 1982).
4. G. LANGDON and F. A. MOHAMED, *J. Mater. Sci.* **11** (1976) 317.
5. R. NOTIS, in "Deformation of ceramic materials", edited by R. C. Bradt and R. E. Tressler, (Plenum Press, New York, London, 1975) pp. 1–22.
6. K. TSUKUMA, M. S. SHIMADA and M. KOIZUMI, *Am. Ceram. Soc. Bull.* **60** (1981) 910.
7. K. NIIHARA and T. HIRAI, *Powder Metall. Int.* **16** (1984) 223.
8. T. EKSTROM and J. PERSSON, *J. Am. Ceram. Soc.* **73** (1990) 2834.
9. T. YAMADA, A. TANAKA, M. SHIMADA and M. KOIZUMI, *Ceram. Int.* **3** (1982) 93.
10. I. TANAKA, G. PEZZOTTI, T. OKAMOTO, Y. MIYAMOTO and M. KOIZUMI, *J. Am. Ceram. Soc.* **72** (1989) 1656.
11. N. UCHIDA, M. KOIZUMI and M. SHIMADA, *Commun. Am. Ceram. Soc.* **68** (1985) C-38.
12. T. DOSDALE and R. J. BROOK, *J. Mater. Sci.* **13** (1978) 167.
13. *Idem, J. Am. Ceram. Soc.* **66** (1983) 392.
14. J. M. VIEIRA and R. J. BROOK, in "Advances in ceramics", Vol. 10, edited by W. D. Kingery (American Ceramic Society, Columbus, OH, 1983) pp. 438–63.
15. C. P. GAZZARA and D. R. MESSIER, *Am. Ceram. Soc. Bull.* **56** (1977) 777.
16. E. F. UNDERWOOD, "Quantitative stereology" (Addison-Wesley, Reading, Palo Alto, London, Don Mills, 1970).
17. G. WOTTING, B. KANKA and G. ZIEGLER in "Non-oxide technical and engineering ceramics", edited by S. Hampshire (Elsevier, London, New York, 1986) pp. 83–94.
18. W. KOLLENBERG and H. SCHNEIDER, *J. Am. Ceram. Soc.* **72** (1989) 1739.
19. J. LANKFORD, *J. Mater. Sci.* **18** (1983) 1666.

20. T. G. NIEH and J. WADSWORTH, *Scripta Metall. Mater.* **24** (1990) 1489.
21. M. G. NAYLOR and T. F. PAGE, Technical Report DA-ERO-78-G-010, Cambridge (1981).
22. R. R. RICE, in "Treatise on materials science and technology," Vol. 11, edited by R. K. MacCrone (Academic Press, New York, 1977) pp. 199–381.
23. P. M. SARGENT and T. F. PAGE, *Proc, Brit. Ceram. Soc.* **26** (1978) 209.
24. S. HAMPSHIRE, R. A. DREW and K. H. JACK, *Commun. Am. Ceram. Soc.* **67** (1984) C-46.
25. D. R. MESSIER and A. BROZ, *ibid.* **65** (1982) C-123.
26. R. F. SILVA, A. P. MOREIRA , J. M. GOMES, A. S. MIRANDA and J. M. VIEIRA, *Mater. Sci. Eng.* **A168** (1993) 55.
27. F. F. LANGE and B. I. DAVIS, *J. Mater. Sci.* **17** (1982) 3637.
28. P. M. SARGENT and M. F. ASHBY, *Mater. Sci. Technol.* **8** (1992) 594.
29. J. A. YEOMANS, PhD dissertation, University of Cambridge, Cambridge, UK (1986).
30. A. G. ATKINS, A. SILVERIO and D. TABOR, *J. Inst. Metals* **94** (1966) 369.
31. T. O. MULHEARN and D. TABOR, *J. Inst, Metals* **89** (1960–61) 7.
32. R. F. SILVA and J. M. VIEIRA, in "Proceedings of the European Ceramic Society 3rd Conference" Vol. 3, edited by P. Duran and J. F. Fernandez (Faenza Editrice Iberica S. L., Castellón de la Plana, 1993) pp. 423–8.
33. R. F. SILVA and J. M. VIEIRA, in "Proceedings of the European Ceramic Society 2nd Conference", Vol. 2, edited by G. Ziegler and H. Hausner (Deutsche Keramische Gesellschaft, Köln, 1993) pp. 817–21.

Received 27 May 1994
and accepted 24 May 1995